Werk

Jahr: 1981
Kollektion: fid.geo
Signatur: 8 Z NAT 2148:50
Digitalisiert: Niedersächsische Staats- und Universitätsbibliothek Göttingen
Werk Id: PPN1015067948_0050
PURL: http://resolver.sub.uni-goettingen.de/purl?PPN1015067948_0050

LOG Id: LOG_0038
LOG Titel: The Romanian earthquake of March 4, 1977 III. Improved focal model and moment determination
LOG Typ: article

Übergeordnetes Werk

Werk Id: PPN1015067948
PURL: http://resolver.sub.uni-goettingen.de/purl?PPN1015067948
OPAC: http://opac.sub.uni-goettingen.de/DB=1/PPN?PPN=1015067948

Contact

Niedersächsische Staats- und Universitätsbibliothek Göttingen
Georg-August-Universität Göttingen
Platz der Göttinger Sieben 1
37073 Göttingen
Germany
Email: gdz@sub.uni-goettingen.de

J Geophys (1982) 50:143–150

Journal of Geophysics

The Romanian Earthquake of March 4, 1977

III. Improved Focal Model and Moment Determination *

E. Räkers [1] ** and G. Müller [2]

[1] Geophysical Institute, University of Karlsruhe, Hertzstr. 16, 7500 Karlsruhe, Federal Republic of Germany
[2] Institute of Meteorology and Geophysics, University of Frankfurt, Feldbergstr. 47, 6000 Frankfurt, Federal Republic of Germany

Abstract. The focal process of the Romanian earthquake of March 4, 1977, which had already been studied in an earlier paper (Müller et al. 1978), is reinvestigated on the basis of additional data from the Russian seismic network. The general features of this multiple event, as given in the first investigation, were confirmed, but several details changed significantly. It is shown that the weak foreshock of this earthquake (depth according to CSEM and ISC 93 and 86 km, respectively) took place at about the same location as the beginning of the main phase of rupture, shock 1. Additional accelerations of rupture which are summarized as shock 2 are difficult to localize with respect to shock 1. Rupture propagated essentially horizontally and towards the SW and terminated abruptly 13 s later at the place of shock 3, about 50 km away from shock 1; this produced exceptionally strong stopping phases in far-field seismograms. The average rupture velocity was 3.7 km/s. A new fault-plane solution is given for shock 1 and an approximate one for shock 3 which indicates significant deviations of the rupture surface from a plane. *P*-wave seismograms of several long-period WWNSS stations are modelled with the aid of theoretical seismograms, using the concept of a station-dependent equivalent moment function of a single double-couple source. The moments determined in this way fall into the range $2\text{–}3 \times 10^{27}$ dyne-cm.

Key words: Earthquakes – Rupture process – Fault-plane solution – Seismic moment

Introduction

In a first study of the Romanian earthquake of March 4, 1977 (Müller et al. 1978, hereafter called paper I) evidence was presented for the multiple nature of this event. The earthquake consisted of a weak foreshock, followed by at least three main shocks (called shocks 1, 2, 3 in the following), whose relative locations were determined by a master-event analysis. A fault-plane solution was derived for shock 1 from long-period seismograms from the Worldwide Network of Standard Seismographs (WWNSS). According to the proposed rupture model, rupture propagated uphill over a distance of about 20 km from the location of the foreshock at a depth of 93 km (source depth according to Centre Séismologique Européo-Méditerranéen (CSEM), to the place of shock 1, where the main phase of the earthquake was initiated about 5 s later. Rupture propagation after this moment was in general directed towards the SW and downhill. A location with acceleration of rupture, shock 2, was located somewhat off the steep, NW-dipping nodal plane of the fault-plane solution. Rupture stopped abruptly and close to this nodal plane at a slant distance of 72 km from, and 14.5 s after, shock 1 at a depth of 109 km (shock 3), producing strong stopping phases in the seismograms.

The purpose of the present paper is to summarize some new aspects of the focal process of the Romanian earthquake which emerged from a detailed analysis of the data of paper I and of additional data from the Russian network of seismic stations (Räkers 1981). We present an improved fault-plane solution for shock 1, put forth evidence for a closer collocation of the foreshock and shock 1 than derived in paper I, redetermine the location of shock 3 relative to shock 1, and discuss briefly the (uncertain) nature of shock 2. Our results on these points represent significant, although not basic, changes of the rupture model suggested in paper I. Moreover, we infer from an approximate fault-plane solution of shock 3 that a rotation of the rupture surface took place during the earthquake, and determine the seismic moment by time-domain modelling of the wave-group consisting of the phases *P*, *pP* and *sP* at several stations. We

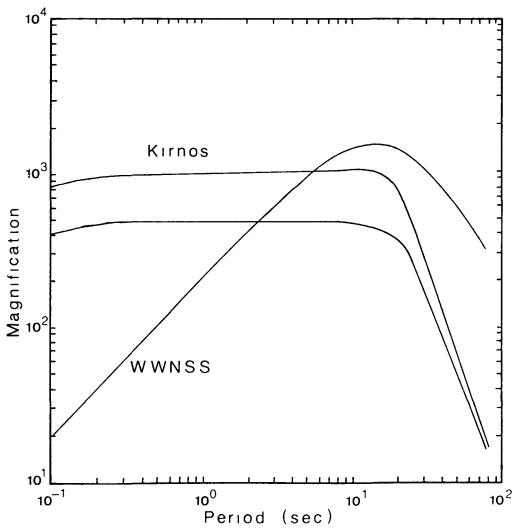

Fig. 1. Typical magnification curves of long-period electrodynamical seismographs in the Russian network (Kirnos instruments) and the Worldwide Network of Standard Seismographs (WWNSS)

* Contribution No. 242, Geophysical Institute, University of Karlsruhe

** *Present address:* Institut für Geophysik, Westfälische Berggewerkschaftskasse, Herner Str. 45, D-4630 Bochum

0340-062X/82/0050/0143/$01.60

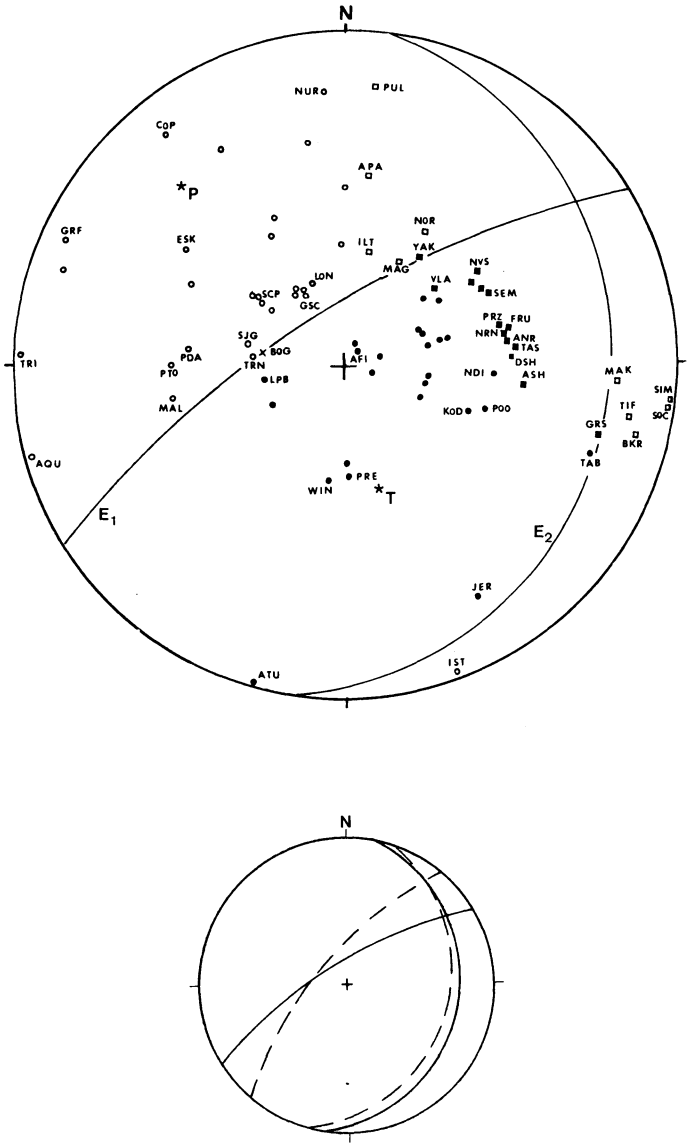

Fig. 2. New fault-plane solution of shock 1 (*top*) and comparison with the old solution (*bottom*). Equal-area projections of the lower focal hemisphere, *open symbols* are dilatations, *closed symbols* compressions

also discuss the focal model which Hartzell (1979) investigated in order to explain the accelerograms of the earthquake recorded at Bucharest.

The following records of the Romanian earthquake were at our disposal:

a) about 60 long-period and a few short-period records from WWNSS stations,

b) long- and short-period records from 28 Russian stations (see Fig. 1 for a comparison of the magnification curves of the most commonly used long-period Kirnos electrodynamic seismographs and a long-period WWNSS instrument),

c) broadband seismograms of the station GRF (Gräfenberg, Federal Republic of Germany),

d) copies of Mainka pendulum records of the Romanian stations BAC, BUC, CMP and IAS.

New Fault-Plane Solution of Shock 1

Figure 2 shows the new fault-plane solution of shock 1, based on long-period WWNSS and Russian data. The essential changes with respect to the fault-plane solution of paper I are a rotation of the strike direction of nodal plane E1 by 18° and an increase of its dip angle by 6°. These changes are required by the downward motions at the Russian stations ILT, MAG and NOR. A reinspection of the WWNSS stations close to nodal plane E1 showed, (1) that the polarities of stations TRN and GSC hat to be changed from upward to downward, (2) that BKS (located close to GSC and LON) had to be omitted because of strong background noise at the expected arrival time of energy from shock 1, and (3) that shock 1 is invisible at BOG, i.e., that BOG is very close to nodal plane E1. (Expected arrival times for shock 1 at BKS and BOG followed from safe readings of this shock at nearby stations, corrected for the travel-time difference due to the difference in epicentral distance.)

The parameters of the new fault-plane solution are:

	Azimuth (deg)	Dip (deg)
Pole of nodal plane E1	148	14
Pole of nodal plane E2	278	69
P-axis	317	24
T-axis	165	57

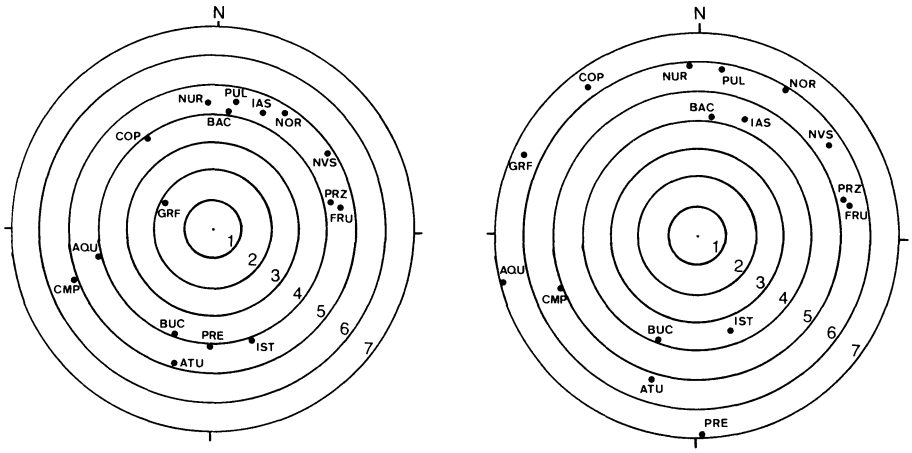

Fig. 3. Travel-time differences in seconds between the foreshock and shock 1 as a function of station azimuth. *Left*: observations. *Right*: theoretical values corresponding to the model in paper I (depth of foreshock: 93 km, depth of shock 1: 79 km, distance: 19.4 km, azimuth foreshock-shock 1: 130°). For discussion see text

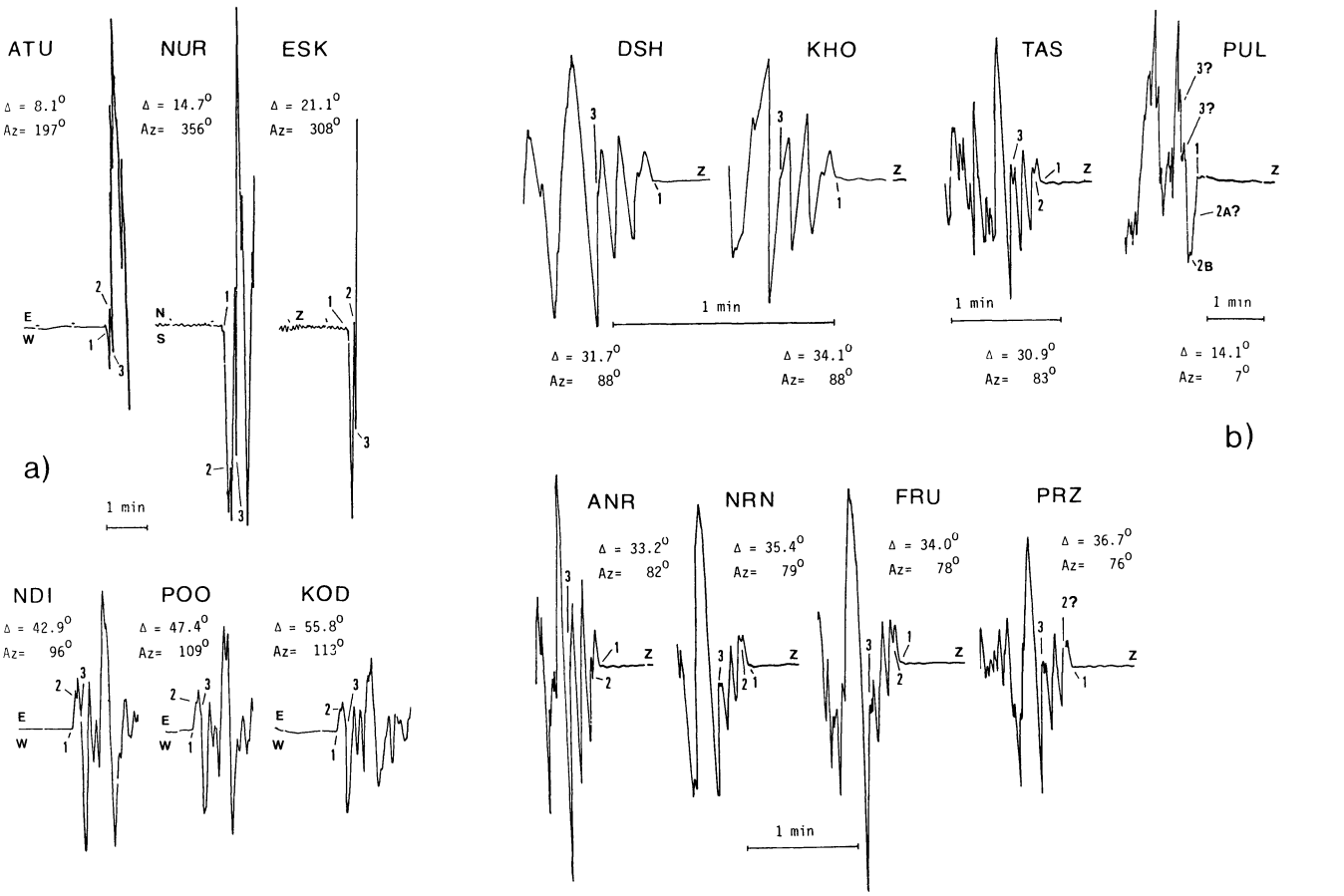

Fig. 4a and b. Long-period seismograms of **a** the WWNSS and **b** the Russian stations that were used in the master-event analysis of shock 3. Note that in the Russian seismograms time increases from right to left and time scales are different. *Numbers* indicate *P* arrivals due to the different shocks

Location of the Foreshock

Figure 3 shows the azimuthal distribution of the observed travel-time differences between shock 1 and the foreshock, together with the distribution of travel-time differences which would be expected if the foreshock location was as suggested in paper I. This model obviously does not satisfy the observations. We do not want to discuss the reasons given in paper I for the choice of the foreshock location, but rather say that the azimuthal distribution of the travel-time differences with values almost exclusively between 4 and 5 s points to the locations of the foreshock and shock 1 being quite close together. The exceptionally low value of the travel-time difference for GRF may be related to the weaker amplitudes of shock 1 at this station, compared with other stations, such that at GRF the noise level masked the foreshock for longer. We disregard the GRF data point because of the rather large number of other observations which are all compatible. Our model, then, is that the foreshock (CSEM coordinates: 26.78 E, 45.78 N, depth 93 km, origin time 19:21:56.2; International Seismological

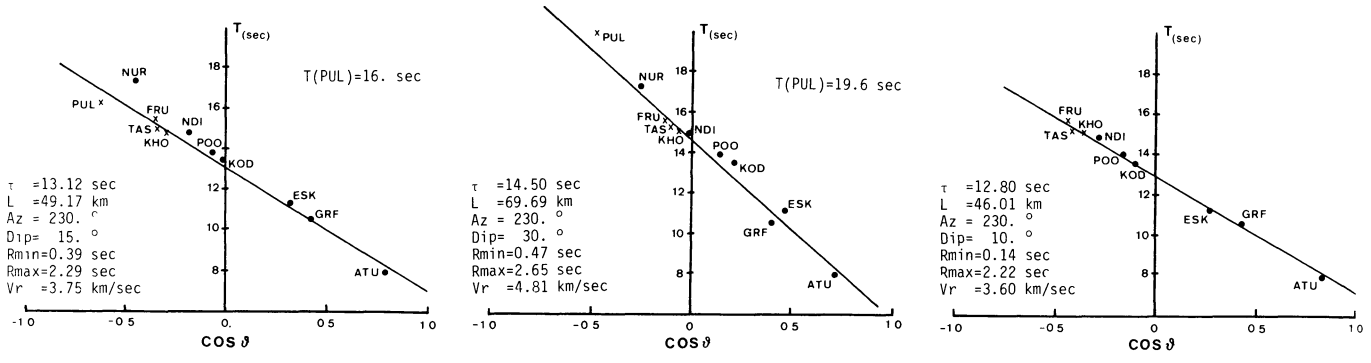

Fig. 5. Master-event analysis for shock 3 relative to shock 1: regression lines for T versus cos ϑ in three different cases. ●=WWNSS stations, x=Russian stations. The Russian stations ANR, DSH, NRN and PRZ are not shown since their data are close to those of FRU, KHO and TAS. Az=azimuth of the direction from shock 1 to shock 3, Dip=dip angle of this direction, R_{min} and R_{max}=minimum and maximum residue, $V_r = L/\tau$=apparent rupture velocity

Centre (ISC) coordinates: 26.72 E, 45.83 N, depth 86 km, origin time 19:21:54.1) and shock 1 occurred at about the same place with a time separation of about 4.5 s.

New Master-Event Analysis for Shock 3

The key role that the broadband record of station GRF played in the identification of shock 3 was described in paper I. In Figure 4 those long-period WWNSS and Russian seismograms are reproduced in which the P arrival due to shock 3 can also be seen. The signatures of the two types of instruments involved are different, but as in the WWNSS seismograms, shock 3 in the Russian seismograms is connected with a strong deflection *opposite* to that of shock 1. The travel-time differences T between shock 3 and shock 1, corrected for the screw-line effect of drum recording if necessary, were used in a master-event analysis, as in paper I. Three regression lines $T=\tau-L\cos\vartheta/\alpha$ are shown in Figure 5 (τ=origin-time difference, L=distance between the two shocks, ϑ=angle between the direction from shock 1 to shock 3 and the direction of the P-wave ray to the station, $\alpha=P$ velocity in the focal volume, assumed here to be 8.3 km/s):

- one regression line for all stations mentioned in Figure 4, plus GRF, assuming T (PUL)=16.0 s (Fig. 5a),
- one for all stations and T (PUL)=19.6 s (Fig. 5b),
- and one with PUL and NUR omitted (Fig. 5c).

The result of Figure 5b comes closest to the results of paper I, but we consider the other two solutions to be closer to reality, since the larger value of T (PUL) is less probable (see Fig. 4). In all three cases the location of shock 3 is very near the nodal plane E1 of the fault-plane solution of shock 1 (Fig. 2), such that we retain the identification of this plane as the rupture plane and the interpretation of shock 3 as an abrupt termination of rupture.

Expressing the new coordinates of shock 3 with respect to those of shock 1 by some numbers, we have the time difference 13 s, the slant distance 50 km, the depth difference 13 km (shock 3 is deeper), the epicentral distance 48 km, the azimuth 230° (from shock 1 to shock 3) and the dip angle 15°. The average

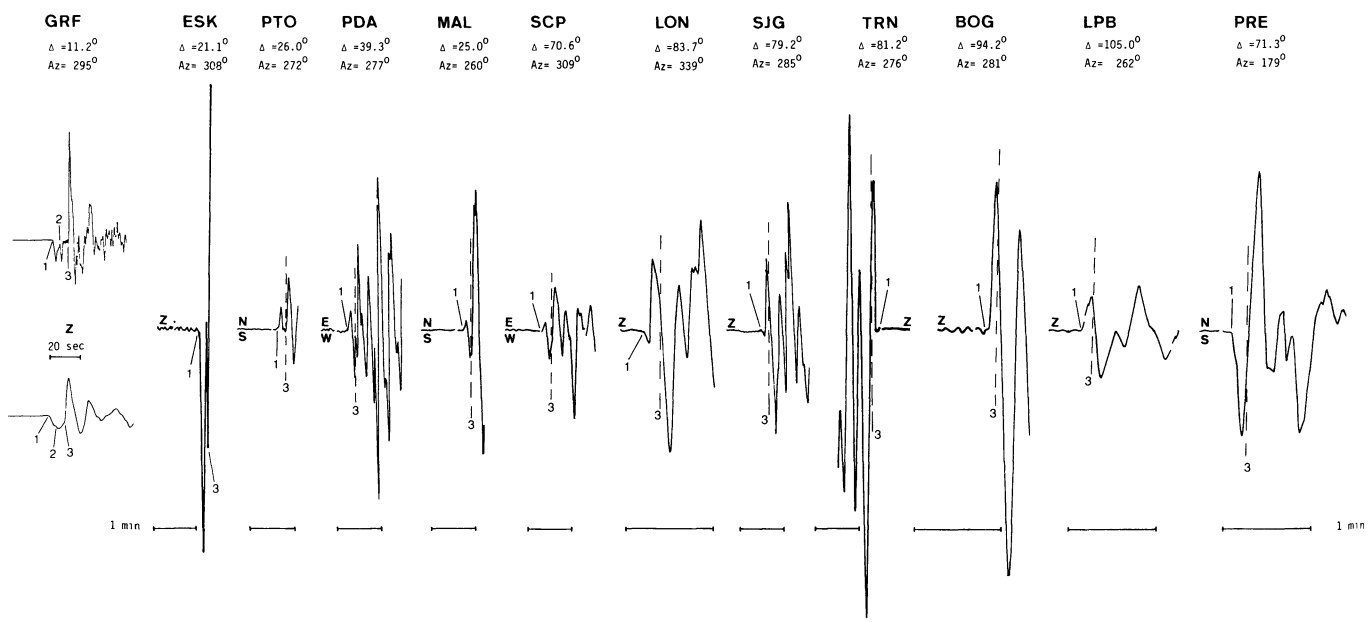

Fig. 6. Seismogram examples showing the polarities of shock 3. The records of GRF (broadband and WWNSS simulation) and ESK, in conjunction with other records (Fig. 4), have been used to predict the shock 3 onset times at stations PTO to PRE, indicated by the *dashed lines*. The shock 3 polarities at these stations correspond to downward motion

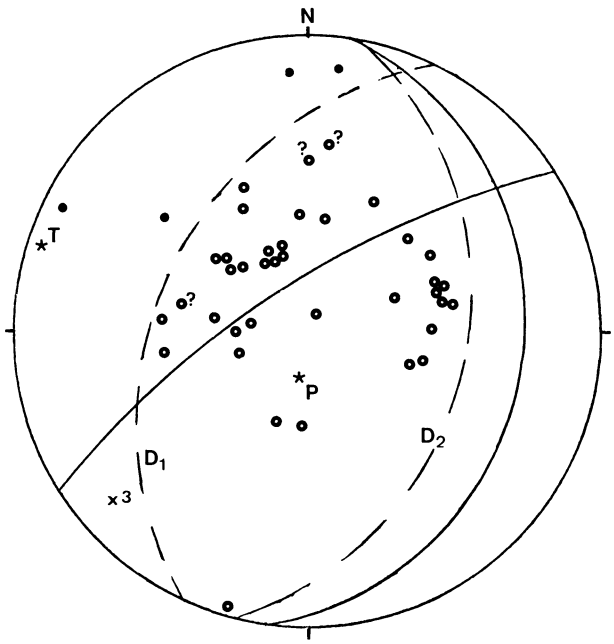

Fig. 7. Approximate fault-plane solution of shock 3 (*dashed nodal lines*), compared with the fault-plane solution of shock 1 (*solid nodal lines*). The cross labelled 3 is the location of shock 3 in the fault-plane solution of shock 1

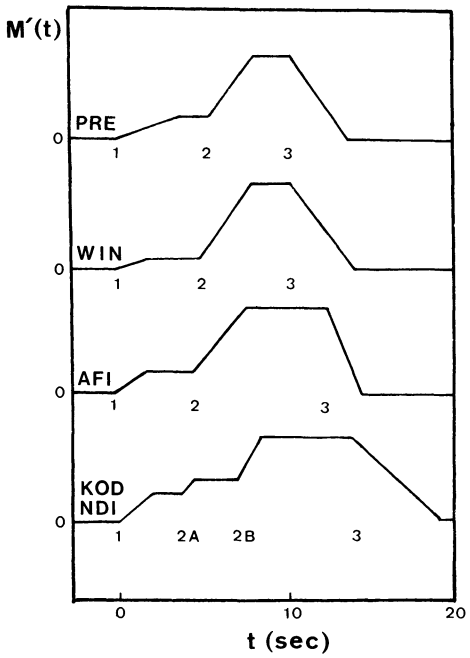

Fig. 9. Moment function time derivatives (normalized) which were used for modelling the long-period records of the WWNSS stations PRE, WIN, AFI, NDI and KOD. The numbers give the times of shocks 1, 2, and 3, as seen by these stations. The form of the curves represents true ground motion

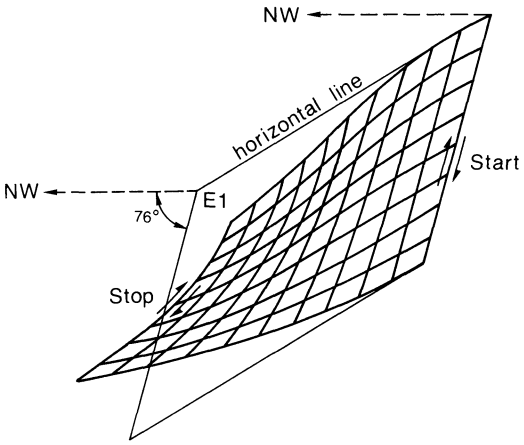

Fig. 8. Schematic diagram, not to scale, of the contorted rupture surface, based on the fault-plane solutions of shock 1 and shock 3. E1 is the initial rupture plane of shock 1

rupture velocity 3.7 km/s is considerably lower than the value 4.98 km/s given in paper I; this is mainly due to the decrease in slant distance from 72 to 50 km. The rupture velocity is about 0.8 times the *S* velocity in the focal region which is assumed to be about 4.6 km/s.

Polarity Distribution for Shock 3

For the identification and localization of shock 3 only those seismograms could be used in which the *P*-wave onset times of this shock could be determined. The polarities of these arrivals could be read in many more records, because shock 3 was so strong. Figure 6 shows examples of seismograms with the expected onset times for shock 3, according to the results of the foregoing section, indicated by dashed lines. The polarities of the deflections following these lines all correspond to dilatational motion. Figure 7 shows a polarity plot in which all useful stations are included. The nodal plane D1 of this approximate fault-plane solution is relatively well determined by the many dilatations and the four safe compressions (at GRF, ESK, PUL and NUR); for nodal plane D2 there is more freedom. The azimuths of the pole directions of D1 and D2 are 115° and 281°, the dip angles 43° and 44°, respectively.

Our interpretation of these polarities is that D1 is the rupture plane of shock 3. Combination with the fault-plane solution of shock 1 indicates that the rupture surface of the whole earthquake deviated considerably from a plane: towards the SW end the rupture surface became less steep and changed its strike direction more towards the N (Fig. 8). These contortions of the rupture surface make it difficult to give a fault-plane solution which is representative for the whole earthquake; this is a certain drawback for the moment determination in a later section.

Re-Investigation of Shock 2

There are a few clear indications that between the shocks 1 and 3 there was an additional shock with rather strong *P*-wave radiation (see the GRF records in Figure 6 and the WWNSS records in Fig. 4a). The corresponding master-event analysis in paper I, however, did not give a very convincing result: the location of shock 2 was quite far off the rupture surface and had great uncertainty. The Russian data (see the examples in Fig. 4b) complicate the matter even more, since they indicate more than one shock between the shocks 1 and 3. We determined the time differences with respect to shock 1 of all onsets between shock 1 and shock 3 in all available seismograms and tried to group them, in order to find out whether shock 2 could possibly consist of two shocks, 2A and 2B (see the record for PUL in Fig. 4b). As a result, we actually consider this a possibility, but of questionable significance, since we probably would

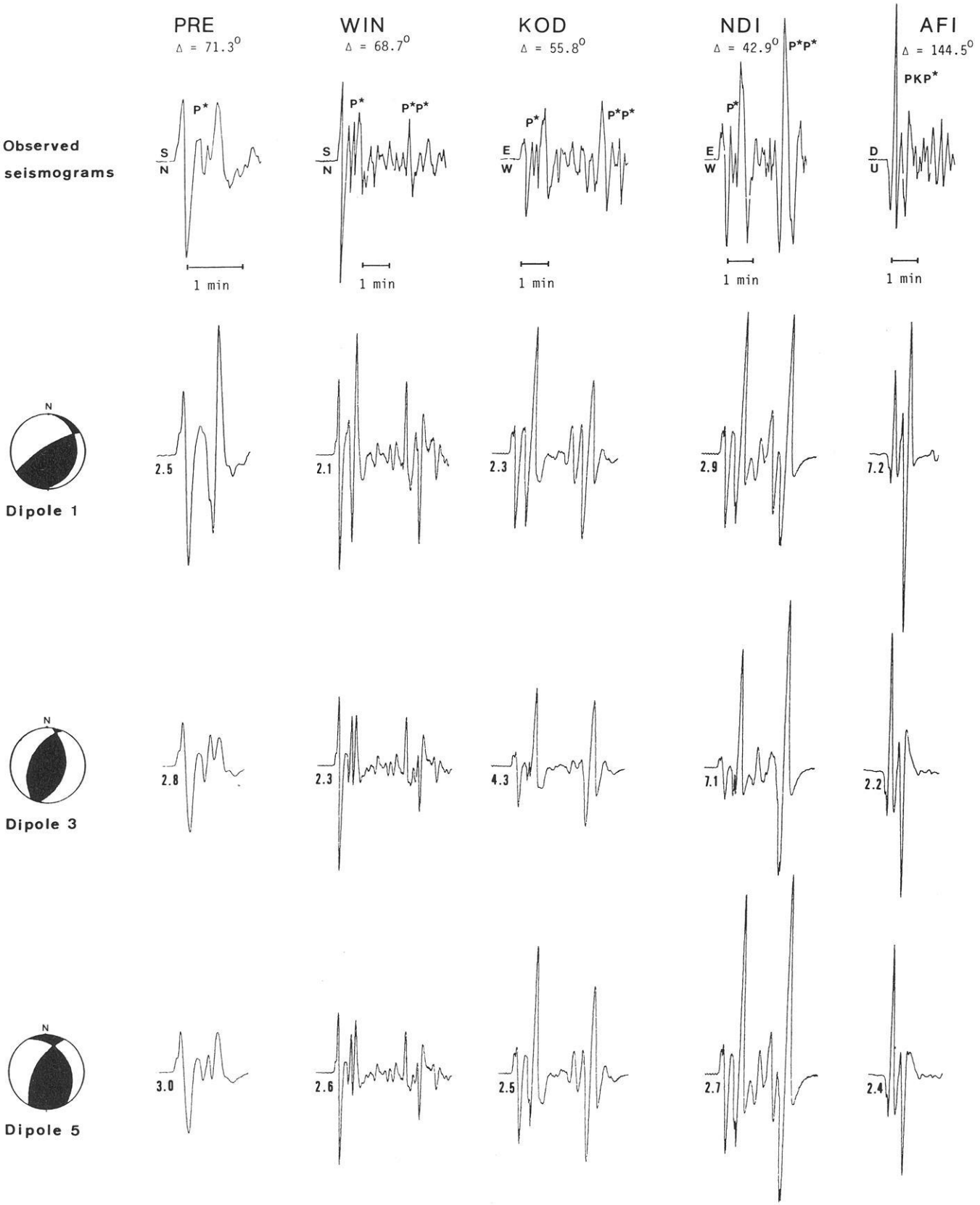

Fig. 10. Comparison of observed and theoretical seismograms for three different double couples. Dipole 1 corresponds to shock 1 (Fig. 2), dipole 3 to shock 3 (Fig. 7) after a change in sign, and dipole 5 is one of a few more orientations investigated. The moment derivatives assumed for each station are shown in Fig. 9. The numbers below the beginning of the theoretical seismograms are the moment values in units of 10^{27} dyne-cm

also have been able to infer more than two shocks. We therefore conclude only that apparently the rupture process between the shocks 1 and 3 was more complex than implied by the model of one additional shock, but that these complexities are not resolvable, at least not with far-field observations.

Moment Determination

Hartzell (1979) has estimated the moment of the Romanian earthquake from surface-wave amplitudes, as recorded by WWNSS, Seismic Research Observatory (SRO) and High Gain Long Period (HGLP) stations, and found a value in the range $1–2 \times 10^{27}$ dyne-cm. The rupture process was modelled by a SW-moving point shear dislocation which had a step moment function and the fault-plane solution of shock 1, as given in paper I. Here, we attempt to model with theoretical seismograms the compressional body-wave phases *P*, *pP* and *sP* which on long-period records form one complicated arrival, called *P** in the following; for one distant station *PKP** is used. Additional to the complexity due to surface reflections is the complexity due to the rupture process itself. We condense this complexity into the moment function of a stationary point-source at a depth of 95 km, i.e., each station which is used in the analysis is assigned an equivalent moment function whose qualitative features – mainly the times of slope discontinuities of the moment derivative–follow from the multiple-event analysis. Another simplifying assumption is that we work with a time-independent orientation of the double couple; it is varied in a few discrete steps between the fault-plane solution for shock 1 (Fig. 2) and the reversed fault-plane solution of shock 3 (Fig. 7). The whole procedure is a rather time-consuming trial and error procedure which, however, gives direct insight into the effects of parameter changes.

The theoretical seismograms were calculated with the reflectivity method for a typical earth model (Model SP-1 of Faber and Müller (1980)). Absorption was approximately taken into account by applying an acausal frequency-domain operator whose value of t^* was assumed to be 0.8 s for all stations. Instrument characteristics were also included. Seismogram modelling was attempted for the WWNSS stations PRE, WIN, NDI, POO, HKC and AFI which were at distances greater than 30° and not too close to the nodal planes of shock 1. Figure 9 shows the normalized moment function derivatives assumed for some of these stations, with the times of shocks 1, 2 and 3 indicated. Integrating these functions gives a gradual build-up of the moment function whose final value, after 15–20 s, is the moment of the earthquake. Theoretical seismograms, calculated for these source functions and three different double-couple orientations, are presented in Figure 10 in comparison with observed seismograms. Matching observed and theoretical seismograms at the first peak-to-peak amplitude gives the moment values indicated below the traces.

The fit of observed and theoretical waveforms in Figure 10 is always good during the first 15–20 s, which confirms the general character of the moment functions and the rupture duration of about 13 s implied by our model. For later times the agreement is of variable quality mainly because of the variable success in modelling the amplitudes of *sP* relative to those of *P*. The amplitude ratio of these two phases depends strongly on the source orientation. In the case of dipole 1 the radiation of *sP* relative to *P* (or of *sPKP* relative to *PKP* for station AFI) is always too strong. For AFI this is due to the fact that this station is relatively close to the *P*-wave nodal plane E1 (see Fig. 2); this leads to an over-estimated moment of 7.2×10^{27} dyne-cm. Disregarding this station, we infer a moment of $2–3 \times 10^{27}$ dyne-cm. In the case of dipole 3 there is, for the stations PRE, WIN and AFI, a considerable improvement of the fit for the *complete* pulses *P** and *PKP**, respectively. The stations KOD and NDI are now too close to the nodal plane D2 (see Fig. 7), such that for these stations there is less agreement of theory and observation than for the other stations. PRE, WIN and AFI point to a moment of $2–3 \times 10^{27}$ dyne-cm and thus support the value obtained for dipole 1. Finally, in the case of dipole 5, which has a roughly intermediate orientation between the dipoles 1 and 3, the success of pulse-form modelling is fair to excellent for all stations, and all moments fall into the range $2.4–3.0 \times 10^{27}$ dyne-cm. A cautious conclusion from these (and several other) modelling experiments, which takes into account the simplifying assumptions that we have made, is that the Romanian earthquake had a moment of $2–3 \times 10^{27}$ dyne-cm. This is somewhat higher than the value $1–2 \times 10^{27}$ dyne-cm, inferred by Hartzell (1979) from surface waves. In view of the uncertainties which enter the moment determination from both body and surface waves, it is probably not justified to consider this as an essential disagreement.

A dipole such as dipole 5 is probably a good average focal mechanism of the Romanian earthquake. For completeness we give the orientation of this dipole: the pole directions of the nodal planes have the azimuths 118° and 240°, and the dip angles 30° and 56°, respectively.

Discussion and Conclusions

The successful modelling of far-field seismograms supports our interpretation of shock 3 as being due to rupture termination at the SW end of the fault zone. Thus, the distance of about 50 km between shock 1 and shock 3, found in the master-event analysis, is a lower limit for the horizontal extent of the rupture surface. The dimension in the dip direction probably is neither larger nor much less than the horizontal dimension. We thus assume fault dimensions of 60 and 40 km, respectively, giving a rupture area of about 2,400 km^2. A rupture surface of this size falls well within the aftershock volume of the earthquake, as determined by Fuchs et al. (1979). For a moment value of 2.5×10^{27} dyne-cm and a rigidity of 7.0×10^{11} dyne/cm^2 in the focal zone we then obtain an average dislocation of about 2.2 m. If we apply the well-known formula for the stress drop on a circular dislocation we find a stress-drop estimate of 52 bar.

Hartzell (1979) studied the accelerograms of the Romanian earthquake, recorded at Bucharest, and compared the displacement records, obtained by integration, with theoretical seismograms, calculated for three different types of source models. His *line-source model*, consisting of a linear array of 11 point sources which are triggered successively over 13 s, comes closest to our rupture model, since the time during which the moment of the earthquake is built up is about the same as in our model. It appears possible that long-period, far-field seismograms calculated for this model (after a change in the orientation of the line source) resemble observed seismograms. Hartzell's *one-point source models*, however, correspond to a rupture duration of onyl about 1 s. These models are able to explain the periods and pulse duration of the Bucharest displacement records, but the long-period far-field seismograms of the earthquake definitely cannot be modelled by them. The same is true for a *two-point source model* by which Hartzell tries to represent in a simple way the multiple nature of the earthquake. The second source, which has the opposite polarity of the first and radiates about 15 s later, is thought to model the termination of rupture (which,

in actuality, it does not do: it models a second, separate and complete earthquake). Since its strength is only 1/4 of the strength of the first source, the additional radiation does not essentially change the seismograms of the one-point source model.

In conclusion, if we try to combine Hartzell's results and ours, it seems possible that a line-source model made up by a pointshear dislocation, moving horizontally over a distance of 50 km from NE to SW with a velocity of about 3.7 km/s, can be found which explains the main features of both near-field and far-field seismograms. The orientation of the shear dislocation and the moment release as functions of time are constrained by our results, but there appears to be enough freedom left in these quantities for a successful modelling of the near-field seismograms.

Acknowledgments. We are grateful to Professor N. Kondorskaya, Institute of Physics of the Earth, Moscow, for making available the records of the Russian seismic network. The computations for this paper were performed at the computing center, University of Karlsruhe. We thank H. Berckhemer, W. Brüstle, S. Faber, and R. Kind for helpful discussions and reading the manuscript, and I. Hörnchen for typing it.

References

Faber, S., Müller, G.: Sp phases from the transition zone between the upper and lower mantle. Bull Seismol. Soc. Am **70**, 487–508, 1980

Fuchs, K., Bonjer, K., Bock, G., Cornea, I., Radu, C., Enescu, D., Jianu, D., Nourescu, A., Merkler, G., Moldoveanu, T., Tudorache, G.: The Romanian earthquake of March 4, 1977. II. Aftershocks and migration of seismic activity. Tectonophysics **53**, 225–247, 1979

Hartzell, S.: Analysis of the Bucharest strong ground motion record for the March 4, 1977 Romanian earthquake. Bull. Seismol. Soc. Am. **69**, 513–530, 1979

Müller, G., Bonjer, K., Stöckl, H., Enescu, D.: The Romanian earthquake of March 4, 1977. I. Rupture process inferred from fault-plane solution and multiple-event analysis. J. Geophys. **44**, 203–218, 1978

Räkers, E.: Untersuchungen zum Bruchvorgang des rumänischen Erdbebens am 4.3. 1977 und Bestimmung des seismischen Moments mit Hilfe von synthetischen Seismogrammen für P-Wellen. Diploma thesis, University of Karlsruhe, 131 p. 1981

Received October 27, 1981; Revised version December 21, 1981
Accepted January 20, 1982